Electronic Supplementary Material (ESI) for ChemComm.

ESI

Combining Ligand-Enhanced Backdonation and Steric Shielding to Stabilize a Mono-substituted Au(I) Carbene

David Vesseur, Karinne Miqueu, and Didier Bourissou*

Content

Materials and methods

All reactions and manipulations were carried out under an atmosphere of dry argon using standard Schlenk techniques or in a glovebox under inert atmosphere. Dry, oxygen-free solvents were employed. All reagents were purchased from Sigma Aldrich. Solution ^{1}H, ^{13}C and ^{31}P NMR spectra were recorded on Bruker Avance 300 or 400 spectrometers at 298 K unless otherwise stated. Chemical shifts (δ) are expressed with a positive sign, in parts per million. ^{1}H and ^{13}C chemical shifts reported are referenced internally to residual protio- (^{1}H; δ 5.32 for CD_2Cl_2) or deutero- (^{13}C; δ 53.84 for CD_2Cl_2) solvent, while ^{31}P chemical shifts are relative to 85% H_3PO_4. The following abbreviations and their combinations are used: br, broad; s, singlet; d, doublet; t, triplet; m, multiplet. The ^{1}H and ^{13}C resonance signals were attributed by means of 2D COSY, HSQC and HMBC experiments. J_{HP} and J_{PC} were determined by comparison with the relevant $^{1}H\{^{31}P\}$ and $^{13}C\{^{1}H,^{31}P\}$ spectra.

Experimental procedures

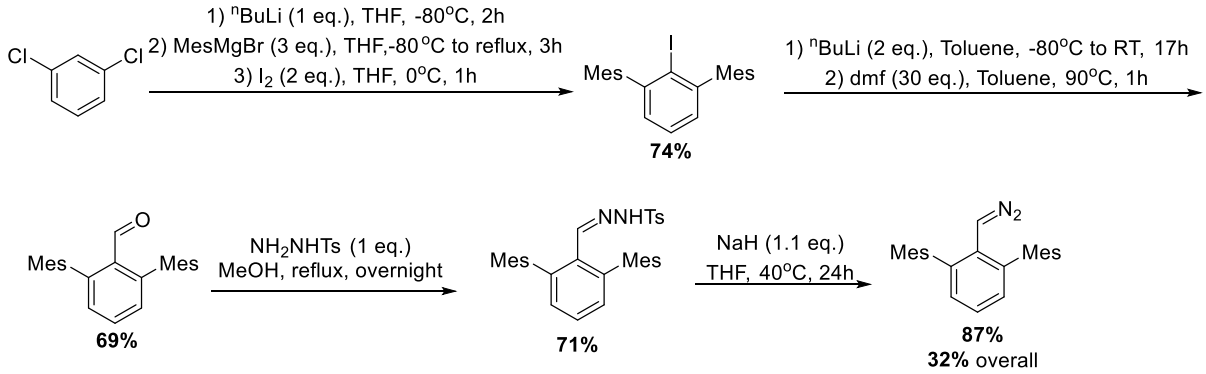

Scheme S1. Synthetic route to $CH(N_2)Dmp$.

Synthesis of DmpI

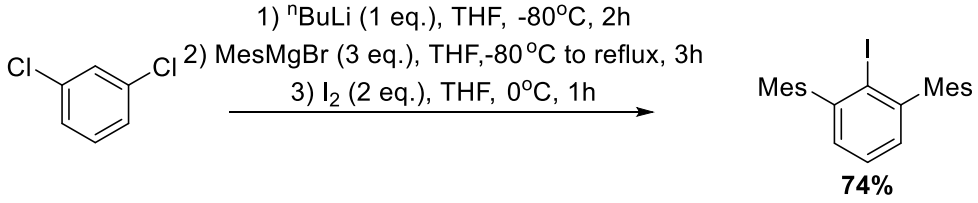

An oven dried three necked flask connected to a reflux condenser and a dropping funnel was flushed with argon (3x). Magnesium powder (1.5 g, 62.7 mmol, 3.0 eq.) was the added to the three necked flask as well as dry THF (15 mL). Mesityl bromide (9.5 mL, 12.54 g, 62.7 mmol, 3.0 eq.) in dry THF (45 mL) was added to the dropping funnel. A small amount of the mesityl bromide and some iodine crystals were added and the mixture was stirred. This caused the mixture to heat slightly after which the rest of the mesityl bromide was added dropwise. The dropping funnel was replaced by a stopper and the mixture was refluxed for 3 hours after which it was allowed to cool to room temperature.

Another oven dried three necked round bottom flask connected to a reflux condenser was flushed with argon (3x). 1,3-dichlorobenzene (3.1 g, 21.1 mmol, 1.0 eq.) and dry THF (50 mL) were added. this was cooled to -80°C in an acetone/nitrogen bath and nBuLi (1.2 mL, 1.6 M in hexanes, 21.1 mmol, 1.0 eq.) was added slowly. This mixture was stirred for 2 hours after which the freshly prepared mesityl magnesium bromide was added via a canula while maintaining a temperature of -80 °C. The mixture was then allowed to warm to room temperature and subsequently refluxed for 3 hours after which it was allowed to cool to room temperature.

The mixture was cooled to 0°C in an ice water bath and iodine (10.6 g, 41.7 mmol, 2.0 eq.) in dry THF (45 mL) was added and stirred for 30 minutes. A saturated solution of Na_2SO_3 was added and the product was extracted with Et_2O (3 x 100 mL). The organic layers were collected and washed with H_2O (3 x 50 mL) and brine (50 mL) this was dried over $NaSO_4$, filtered and concentrated. The resulting solid was refluxed in EtOH (50 mL) for 30 minutes after which it was cooled to room temperature to give colourless crystals, filtering gave DmpI in a 6.9 gram yield (74%). The spectra matched those reported in literature.[1]

^{1}H NMR (300.11 MHz, $CDCl_3$): 7.46 (t, J^{HH} = 7.5 Hz, 1H), 7.08 (d, J^{HH} = 7.5 Hz, 2H), 6.96 (s, 4H), 2.35 (s, 6H), 1.98 (s, 12H)

Synthesis of CHODmp

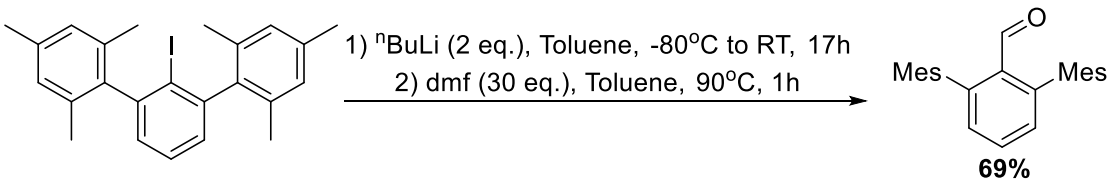

69%

DmpI (2.0 g, 4.5 mmol, 1.0 eq.) was added to a Schlenk and purged with argon (3x). Dry Toluene (20 mL) was added and the mixture cooled to -80 °C in an acetone/nitrogen bath. ^{n}BuLi (5.7 mL, 1.6M in hexanes, 9.1 mmol, 2.0 eq.) was then added dropwise while stirring. The reaction was stirred for 1 hour at -80 °c in a acetone/nitrogen bath after which it was warmed to room temperature and stirred for another 16 hours resulting in a yellow suspension. The mixture was cooled to -80°C in an acetone/nitrogen bath and dry dmf (1.9 g, 2 mL, 138.0 mmol, 30 eq.) was added dropwise. The reaction was warmed to room temperature and stirred for 30 minutes after which it was heated to 90°C and stirred for one hour to give a colourless solution with a white suspension. The mixture was cooled to 0°C in a ice water bath and distilled H_2O (25 mL) was added to quench. The product was extracted with Et_2O (2x 25 mL). The organic fractions were combined and washed with H_2O (3x 25 mL) and brine (25 mL) then dried over $NaSO_4$, filtered and concentrated to give a yellow solid which was dissolved in a minimal amount of pentane at 30°C. Cooling the mixture to -25 °C in a fridge gave a white precipitate. Filtering gave the product as an off white solid in a 1.08 gram yield (69%). The spectra matched those reported in literature.[2]

^{1}H NMR (300.11 MHz, $CDCl_3$): 9.66 (s, 1H), 7.66 (t, J^{HH} = 7.6 Hz, 1H), 7.17 (d, J^{HH} = 7.6 Hz, 2H), 6.94 (s, 4H), 2.34 (s, 6H), 1.96 (s, 12H)

Synthesis of CH(NNHTs)Dmp

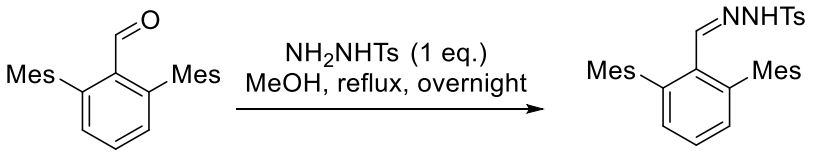

71%

CHODmp (1.08 g, 3.2 mmol, 1 eq.) and $TsNHNH_2$ (596 mg, 3.2 mmol, 1 eq.) were added to a 20 mL round bottom flask and MeOH (6 mL) was added. This mixture was refluxed overnight and cooled to -25 °C in a fridge for several hours to give white crystals. This was filtered and washed with precooled -25°C MeOH (2 x 4 mL) and pentane (2 x 20 mL) to give the product as white crystals in a 1.14 g yield (71%).

^{1}H NMR (300.13 MHz, $CDCl_3$): 7.43 (t, J^{HH} = 7.9 Hz, 1H), 7.32 (d, J^{HH} = 8.6 Hz, 2H), 7.20 (m, 3H), 7.04 (d, J^{HH} = 7.6 Hz, 2H), 6.89 (s, 4H), 2.42 (s, 3H), 2.33 (s, 6H), 1.87 (s, 12H)

Synthesis of $CH(N_2)Dmp$

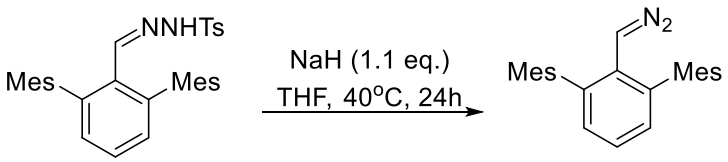

87%

CH(NNHTs)Dmp (511 mg, 1.0 mmol, 1 eq.) was dissolved in THF (10 mL) and slowly added to a stirring suspension of NaH (27.8 mg (95%), 1.1 mmol, 1.1 eq) in THF (5 mL) which resulted in immediate formation of gaseous H_2. This was stirred overnight at 40°C to give a strongly orange coloured solution. The solvent was removed by evaporation and the product was extracted via canula filtration with pentane (4 x 5 mL) till only a white solid remained. The solution was concentrated to approximately half the original volume and stored overnight in a -80°C fridge resulting in the formation of crystals. The pentane was removed via canula filtration giving the product as an salmon coloured solid in a 352 mg yield (8 7%). The spectra matched those reported in literature.[2]

^{1}H NMR (300.11 MHz, CD_2Cl_2): 7.16 (dd, J^{HH} =7.1 Hz, J^{HH} = 8.0 Hz, 1H), 6.96 (d, J^{HH} = 7.5 Hz, 2H), 6.92 (s, 4H), 4.16 (s, 1H), 2.31 (s, 6H), 2.01 (s, 12H)

Synthesis of $(PP)AuNTf_2$

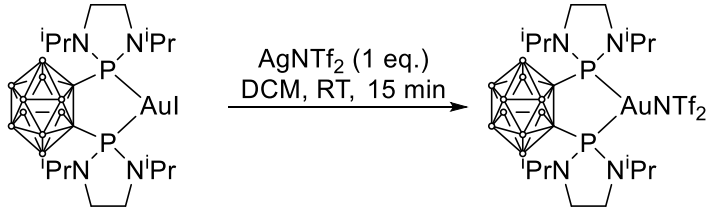

◦ = BH ◦ = BH

85%

In a glove box (PP)AuI (400 mg, 0.49 mmol, 1.0 eq.) and $AgNTf_2$ (191 mg, 0.49 mmol, 1.0 eq.) were added to an aluminium covered vial containing a stirring bar. DCM (10 mL) was added and the reaction was stirred for 15 minutes. The solution was filtered over a short celite pad and washed with DCM (2 x 2mL). The solution was concentrated to approximately half the original volume and stored in a -24°C fridge resulting in the formation of yellow crystals. The solvent was removed by canula filtration, drying under high vacuum gave the product as yellow crystals in a 404 mg yield (85%). The spectra matched those reported in literature.[3]

Generation of **1**

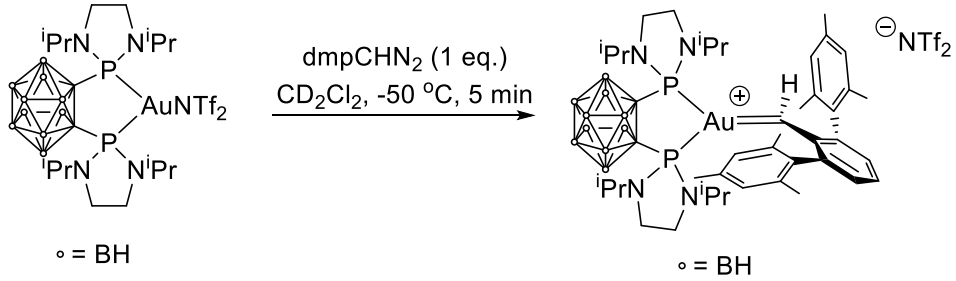

In a glovebox CH(N_2)Dmp (11.0 mg, 0.031 mmol, 1 eq.) and CD_2Cl_2 (0.3 mL) were added to a NMR tube after which it was capped with a septum. (PP)AuNTf_2 (30.0 mg, 0.031 mmol, 1 eq.) and CD_2Cl_2 (0.5 mL) were added to a vial. The solution was taken up into a syringe and the needle was capped with a septum. Outside the glovebox, the NMR tube was cooled to -50°C in a acetone/nitrogen bath after which the solution containing (PP)AuNTf_2 was slowly added to the NMR tube resulting in a direct colour change to deep purple. The NMR tube was then thoroughly sealed with Teflon tape and parafilm after which the tube was completely submerged in the -50°C acetone/nitrogen bath. The tube was allowed to cool for 10 minutes after which it was vigorously shaken for several minutes while maintaining the low temperature. The tube was then transferred to a -80°C acetone/nitrogen bath for transport. Finally, the NMR tube was inserted into a precooled -80°C NMR spectrometer showing clean and quantitative formation of **1**. The complex was fully characterized with multinuclear NMR at this temperature.

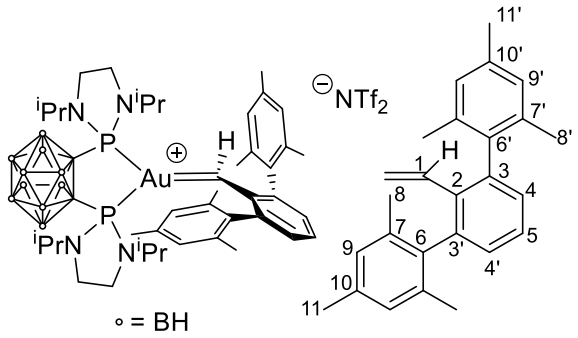

^{1}H NMR (400.13 MHz, CD_2Cl_2, -80°C): 13.36 (t, J^{HP} = 16.6 Hz, 1H, **H_1**), 8.06 (m, 1H, **H_5**), 7.25 (br, 1H, **H_4** or **$H_{4'}$**), 7.18 (bs, 1H, **H_4** or **$H_{4'}$**), 6.94 (bs, 4H, **H_9** and **$H_{9'}$**), 3.45-2.94 (m, 12H, NC**H**$(CH_3)_2$ and N(CH_2C**H**$_2$)N), 2.29 (br, 3H, **H_{11}**), 1.85 (br, 3H, **H_7** or **$H_{7'}$**), 1.85 (br, 3H, **H_7** or **$H_{7'}$**), 1.26 (d, J^{HH} = 6.2 Hz, 6H, NCH(C**H**$_3$)$_2$), 1.19 (d, J^{HH} = 6.2 Hz, 6H, NCH(C**H**$_3$)$_2$), 1.11 (d, J^{HH} = 6.2 Hz, 6H, NCH(C**H**$_3$)$_2$), 0.70 (d, J^{HH} = 6.2 Hz, 6H, NCH(C**H**$_3$)$_2$)

Note: due to overlap with the methyl signals of **8** and **11** and their broadness, the B**H** signals of the carborane could not be assigned.

^{13}C{^{1}H} NMR (100.63 MHz, CD_2Cl_2, -80°C): 295.6 (t, J^{CP} = 85.6 Hz, **C_1**), 154.9 (br, **C_3** or **$C_{3'}$**), 149.3 (t, J^{CP} = 8.9 Hz, **C_2**), 146.5 (br, **C_3** or **$C_{3'}$**), 142.6 (t, J^{CP} = 7.4 Hz, **C_5**), 138.0 (br, **C_7** or **$C_{7'}$** or **C_{10}** or **$C_{10'}$**), 136.7 (br, **C_7** or **$C_{7'}$** or **C_{10}** or **$C_{10'}$**), 136.2 (s, **C_6**), 134.9 (br, **C_7** or **$C_{7'}$** or **C_{10}** or **$C_{10'}$**), 133.4 (br, **C_7** or **$C_{7'}$** or **C_{10}** or **$C_{10'}$**), 131.7 (br, **C_4** or **$C_{4'}$**), 130.3 (br, **C_4** or **$C_{4'}$**), 128.4 (br, **C_9** or **$C_{9'}$**), 127.6 (br, **C_9** or **$C_{9'}$**), 119.0 (q, J^{CF} = 321.1 Hz, N(SO_2C**F**$_3$)$_2$), 91.5 (d, J^{CP} = 62.1 Hz, **C**arborane), 48.8 (m, N**C**H$(CH_3)_2$), 41.9 (s, N(CH_2C**H**$_2$)N), 40.1 (s, N(CH_2C**H**$_2$)N), 23.2 (s, NCH(C**H**$_3$)$_2$), 21.6 (s, NCH(C**H**$_3$)$_2$), 20.6 (m, **C_8**, **$C_{8'}$**, **C_{11}** and NCH(C**H**$_3$)$_2$), 17.0 (s, NCH(C**H**$_3$)$_2$)

^{31}P{^{1}H} NMR (161.98 MHz, CD_2Cl_2, -80°C): δ 141.3 (s)

^{31}P NMR (161.99 MHz, CD_2Cl_2, -80°C): δ 141.6 (broadened s)

^{11}B NMR (128.38 MHz, CD_2Cl_2, -80°C): δ 50 to -50 (br)

Figure S0. Picture of complex 1 in CD2Cl2 seconds after taking it out of a -80 ° Cacetone/nitrogen bath. Left: picture taken with flash. Right: picture without flash.

Variable temperature NMR of **1**

1 was prepared according to the above described procedure. After insertion into a precooled -80°C spectrometer, the temperature was increased in steps of 10°C. After reaching a stable temperature approximately 5 minutes were waited after which the ^{1}H and ^{31}P NMR spectra were measured. When 0°C was reached, the characteristic triplet around 13 ppm had almost entirely disappeared signalling decomposition at this temperature and the experiment was stopped.

Computational details

All calculations were performed using the Gaussian 09 package[4] and the B3PW91 hybrid functional[5] on the different gold carbene complexes. The gold atom was described with the relativistic electron core potential SDD and associated basis set,[6] augmented by a set of f-orbital polarization functions.[7] The 6-31G** basis set was employed for all other atoms.[8] Frequency calculations were undertaken to confirm the nature of the stationary points, yielding zero imaginary frequency for *minima*. All the geometrical structures were plotted with Chemcraft program.[9]

The bonding situation in all systems was studied using Natural Bond Orbital[10] analyses (NBO, 7.0 version).[11] Charge transfer between the carbene and the metallic fragment has been calculated using atomic NPA charges. The Natural Localized Molecular Orbitals (NLMO) associated to the interactions involving the vacant of the carbene, *i.e.* the $d_{xz}(Au) \rightarrow 2p^{\pi}(C_{carbene})$ and $\pi_{C=CAr} \rightarrow 2p^{\pi}(C_{carbene})$ interactions, have been analyzed. NLMO plots associated to the $Au \rightarrow C_{carbene}$ back-donation or $Aryl \rightarrow C_{carbene}$ interaction were drawn (cutoff: 0.04) with Chemcraft program.[9]

For each system, a charge decomposition analysis (CDA) was carried out with the CDA 2.2 program developed by G. Frenking.[12] The orbital contributions to the charge distributions are divided into four parts: *(i)* the mixing of the occupied orbitals of the ligand (carbene) and the unoccupied MOs of the metal fragment L_nAu^+ (Ligand⟶Au donation *d*), *(ii)* the mixing of the unoccupied orbitals of the ligand and the occupied MOs of the metal fragment (Ligand⟵Au back-donation *b*), *(iii)* the mixing of the occupied orbitals of the ligand and the occupied orbitals of the metal fragment (Ligand⟷Au repulsive polarization *r*), and *(iv)* the mixing of the unoccupied orbitals of the ligand and the unoccupied orbitals of the metal fragment (residual term Δ).

Energy Decomposition Analysis[13] was performed with Amsterdam Density Functional program, version 2021.102[14] at ZORA-B3LYP/TZ2P level of theory on the geometry optimized from Gaussian 09 at B3PW91/SDD+f(Au),6-31G** level of theory. Different fragmentations were considered : i) $(P,P)Au^+$(Singlet)/CHR(Singlet), $(P,P)Au^+$(Triplet)/CHR(Triplet) and $(P,P)Au^{3+}/CHR^{2-}$. This analysis is based on the EDA method of Morokuma and the ETS partitioning scheme of Ziegler and Rauk. The interaction energy term $\Delta E_{int}(\zeta)$ is decomposed into different chemically meaningful contributions: (i) electrostatic interaction energy between the reagents (ΔV_{elstat}), (ii) Pauli repulsion which account for destabilizing interactions between occupied orbitals of each fragment (ΔE_{Pauli}), and (iii) stabilizing orbital interactions (ΔE_{orb}).

$$\Delta E_{int} = \Delta V_{elstat} + \Delta E_{Pauli} + \Delta E_{orb}$$

The main orbital interaction contributions to the total ΔE_{orb} term can visualized and quantified by means of the Natural Orbital for Chemical Valence (NOCV)[15] extension of the EDA method. The EDA-NOCV approach is a powerful tool to quantitatively analyze chemical bonds, combining the extended transition state (*ETS*) method for energy decomposition *analysis* combined with the natural orbitals for chemical valence (*NOCV*) theory. Within this methodology, the ΔE_{orb} term is decomposed into the contributions from different natural orbitals of chemical valence (NOCV) eigenvalues (λ_i) as follows:

$$\Delta E_{orb} = \sum_{k} \Delta E_{orb}^{k} = \sum_{k=1}^{M/2} v_k [-F_{-k,-k}^{TS} + F_{k,k}^{TS}]$$

Where the terms $F^{TS}_{k,k}$ are the diagonal Kohn-Sham matrix elements corresponding to NOCVs. The components ΔE^{k}_{orb} provide energetic estimation of $\Delta\rho^k$ and allow to characterize the importance of a particular electron flow channel for the bonding between considered molecular fragments.

Figure S1. Plots of the HOMO and LUMO (cutoff: 0.05) for the **(P,P)AuCH(R)**$^{+}$ complexes, **A-Ph**, **A-Mes** and **A-Dmp**, calculated at the B3PW91/SDD+f(Au), 6-31G**(other atoms) level of theory. H have been omitted for clarity, excepted the H on the carbene center. HOMO-LUMO energy difference (ΔE) in eV.

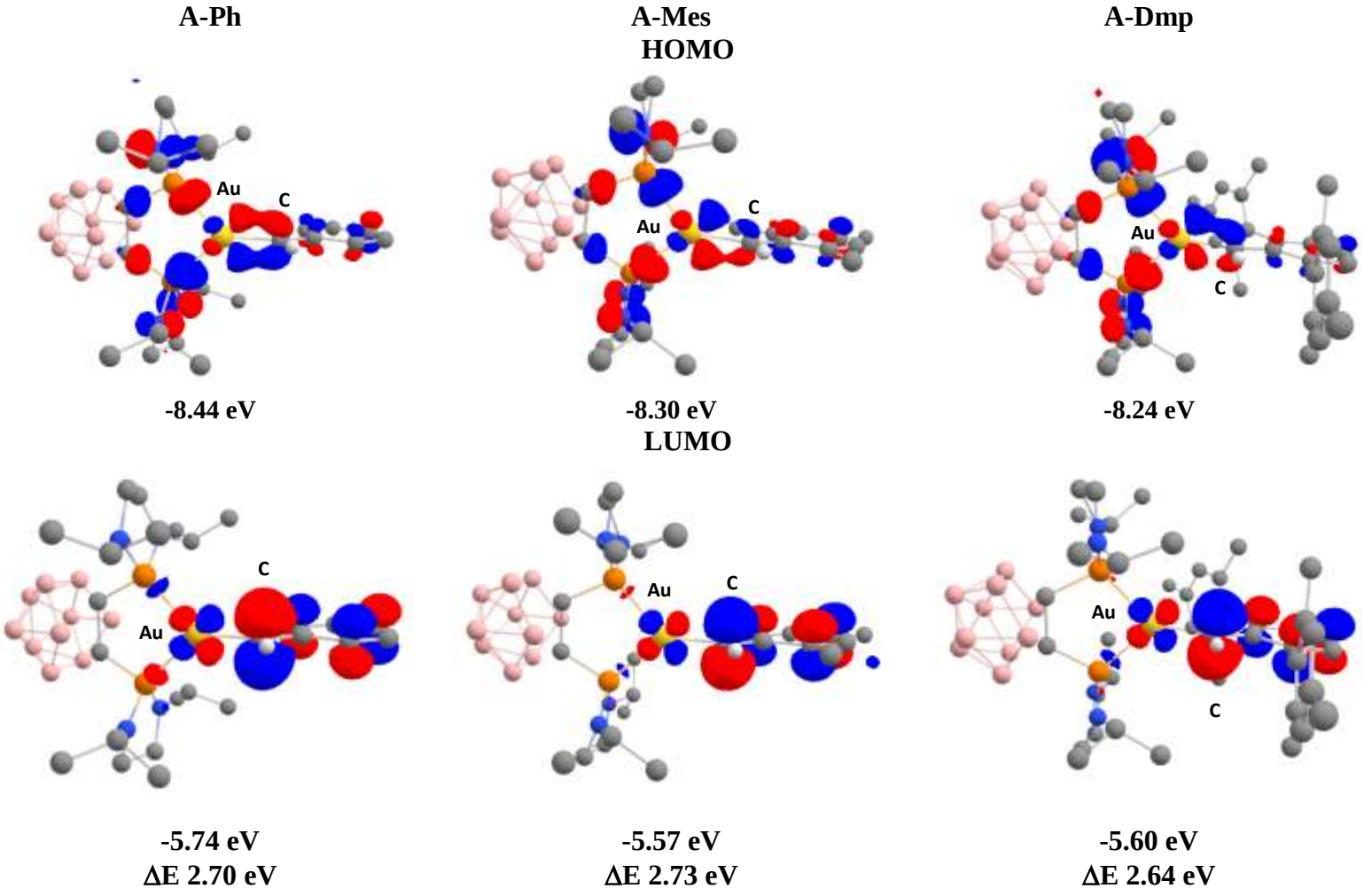

Table S2. CDA analysis for the complexes **A-Ph**, **A-Mes**, **A-Dmp** and for the (**JohnPhos)AuCHMes**$^+$ complex **B-Mes**, calculated at the B3PW91/SDD+f(Au),6-31G**(other atoms) level of theory.

L_2Au^+ (singlet)/**CHR** (singlet)				
	A-Ph	**A-Mes**	**A-Dmp**	**B-Mes**
$CR_2 \rightarrow AuL_2$ donation (d)	0.365	0.447	0.482	0.391
$Au \rightarrow CR_2$ back-donation (b)	0.219	0.215	0.231	0.119
d/b ratio	1.67	2.08	2.09	3.29
Au ↔ C repulsion	-0.348	-0.355	-0.380	-0.356
Residue term (Δ)	0.006	-0.006	-0.006	-0.009

In light of the EDA results (see Table S4), the CDA analysis was carried out in the best fragmentation, *i. e.* L_nAu^+/CHR fragments (both in the singlet state).

Figure S2. Plots of the NLMO (cutoff: 0.04) associated to the donation $C_{carbene} \rightarrow Au$ ($n_C^{\sigma}(C) \rightarrow Au$), the back-donation $Au \rightarrow C_{carbene}$ ($d_{xz}(Au) \rightarrow 2p^{\pi}(C)$) and the delocalization of the aryl group on the vacant of the carbene ($\pi_{C=CAr} \rightarrow 2p^{\pi}(C)$) for complexes **A-Ph**, **A-Mes** and **A-Dmp**. Contributions of gold, $C_{carbene}$ and C_{aryl} atoms in percent. H have been omitted for clarity, excepted the H on the carbene center.

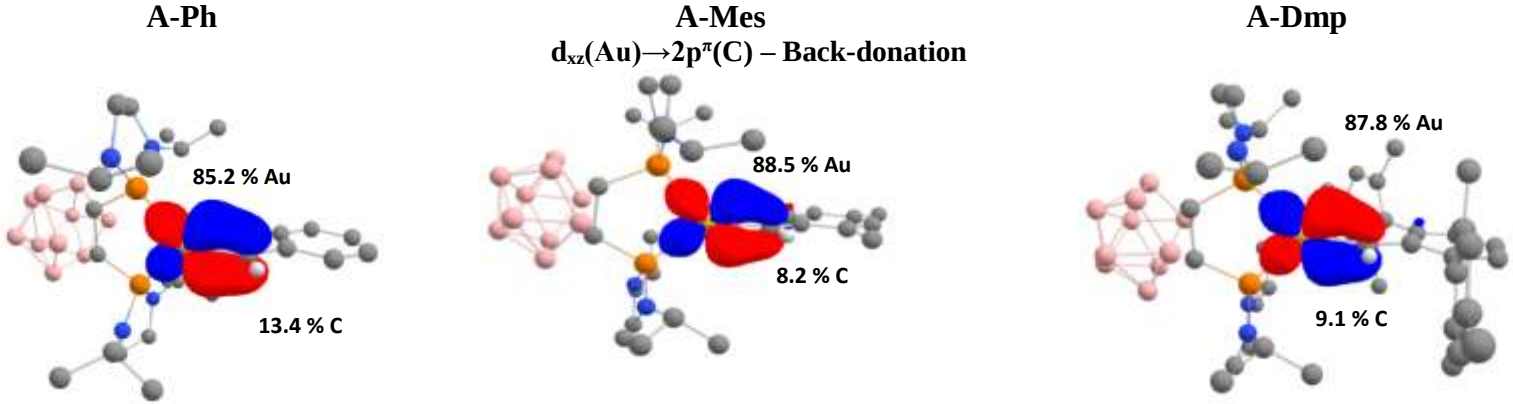

$\pi_{C=Caryl} \rightarrow 2p^{\pi}(C)$

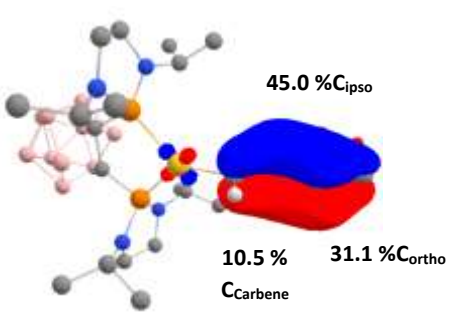

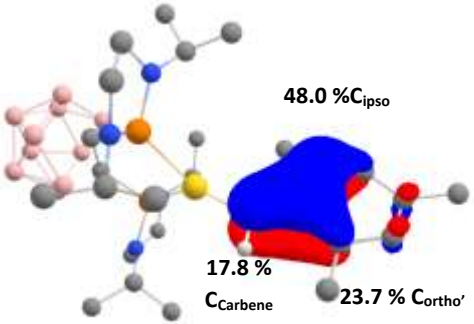

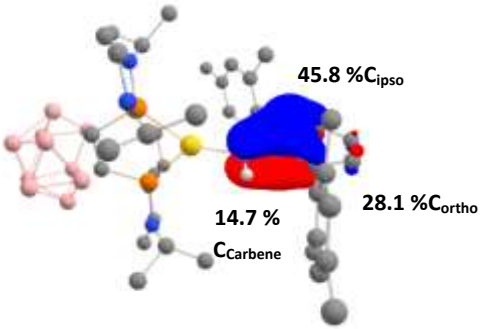

$n_C^{\sigma}(C) \rightarrow$ Au – Donation

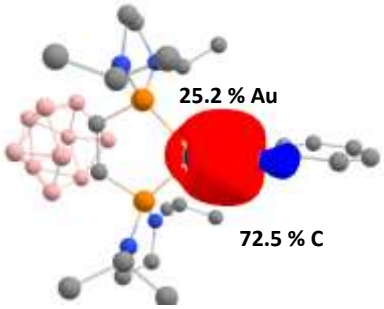

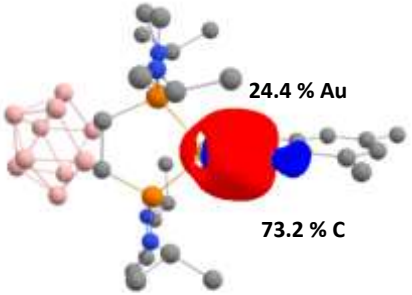

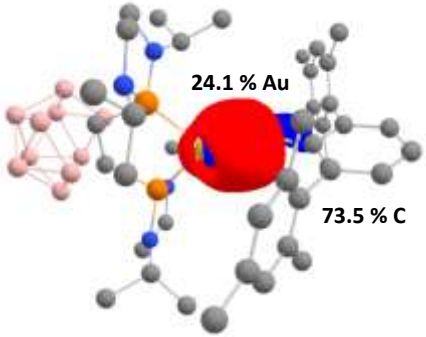

Figure S3. Plots of the main molecular orbitals (cutoff: 0.05) for the (**JohnPhos)AuCHMes**$^{+}$ complex **B-Mes**, calculated at the B3PW91/SDD+f(Au), 6-31G**(other atoms) level of theory. H have been omitted for clarity, excepted the H on the carbene center. Plot of the NLMOs (cutoff: 0.04) associated to the donation $C_{carbene}$→Au (n_C^{σ}(C) → Au), the back-donation Au→$C_{carbene}$ (d_{xz}(Au)→$2p^{\pi}$(C) and to the delocalization of the aryl group on the vacant of the carbene ($\pi_{C=CAr}$→$2p^{\pi}$(C)). Contributions of gold, $C_{carbene}$ and C_{aryl} atoms in percent. H have been omitted for clarity.

HOMO-7

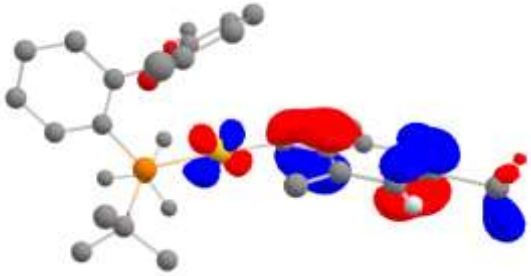

-10.29 eV

HOMO-1

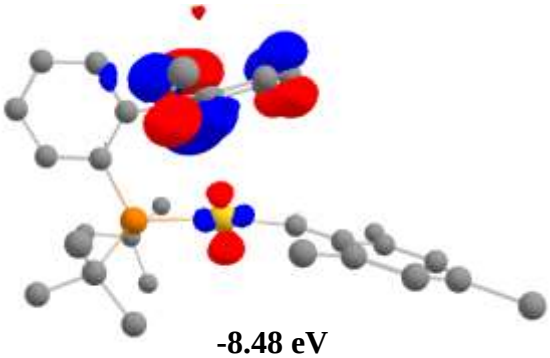

-8.48 eV

LUMO

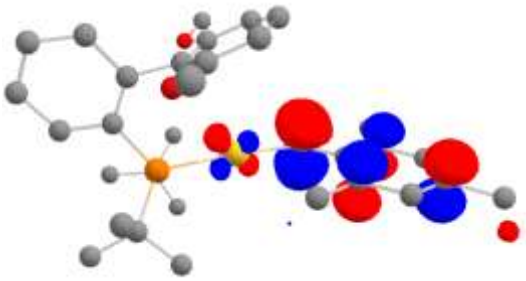

-6.12 eV

NLMO Au→$C_{carbene}$

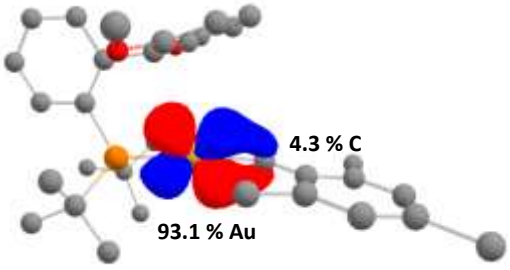

NLMO $\pi_{C=CAr}$→$2p^{\pi}$(C)

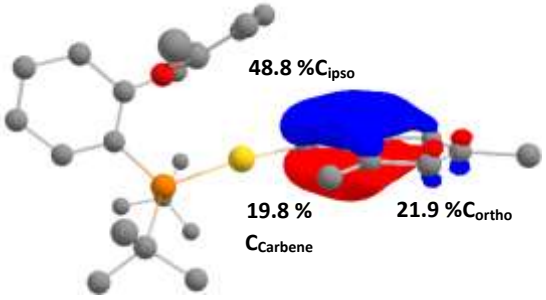

NLMO $C_{carbene}$→Au

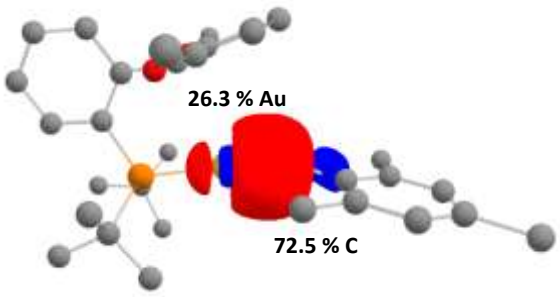

The plot of the main MOs, the NLMOs associated to back-donation Au→$C_{carbene}$ (d_{xz}(Au)→$2p^{\pi}$(C) and to the delocalization of the aryl group on the vacant of the carbene ($\pi_{C=CAr}$→$2p^{\pi}$(C)) as well as the contributions of Au, Ccarbene and C-aryl in these NLMOs confirm the weaker Au→C_{carb} backdonation and stronger Ar→C_{carb} π-donation in **B-Mes** than in **A-Dmp**.

Analysis of the NLMO associated to the donation term ($C_{carbene}$→Au) evidences that this contribution is relatively similar in all gold carbene complexes, meaning that that the difference in stability is not due to the σ-donor effect of the ligand. The main difference comes from the back-donation term.

Table S3. EDA carried out at ZORA-B3LYP/TZ2VP for the complex **A-Dmp** with different fragmentations. Energies are in kcal/mol.

	$(P,P)Au^{+}$ (S)/CHR (S)	**$(P,P)Au^{3+}/CHR^{2-}$**	**$(P,P)Au^{+}$ (T)/CHR (T)**
ΔE_{Pauli}	262.3	334.17	203.19
ΔV_{elstat}	-243.63 (70.1 %)[a]	-648.87	-156.44
ΔE_{orb}	-103.75 (29.9 %)[a]	-358.79	-153.75
ΔE_{int}	-85.10	-673.50	-107.00
	[a] Values into bracket (%) correspond to the percentage contribution to the total attractive interaction (ΔE_{elstat} + ΔE_{orb}).		

We carried out Energy Decomposition Analyses (EDA) using different fragmentations. According to the orbital interaction, the best description for **A-Dmp** is found for the fragmentation $(P,P)Au^{+}$(singlet)/CHR(singlet) rather than $(P,P)Au^{+}$(triplet)/CHR(triplet) or $(P,P)Au^{3+}/CHR^{2-}$.

Table S4. EDA carried out at ZORA-B3LYP/TZ2VP for the complex **A-Ph**, **A-Mes**, **A-Dmp** and **B-Mes**. Only the best fragmentation (P,P)Au^+(Singlet)/CHR(Singlet) has been considered. Energies are in kcal/mol.

	A-Ph	**A-Mes**	**A-Dmp**	**JohnPhosAu$^+$/CHR**
ΔE_{Pauli}	275.95	268.38	262.30	230.22
ΔV_{elstat}	-260.03 (71.7%)[a]	-254.09 (72.0%)[a]	-243.63 (70.1 %)[a]	-231.48 (74.8 %)[a]
ΔE_{orb}	-102.76 (28.3%)[a]	-99.04 (28.0 %)[a]	-103.75 (29.9 %)[a]	-78.07 (25.2 %)[a]
ΔE_{int}	-86.84	-84.76	-85.10	-79.34
ΔE_{orb1} (ρ)	-50.7 (back-donation)	-49.9 (Donation)	-49.6 (Donation)	-44.7 (Donation)
ΔE_{orb2} (ρ)	-34.6 (back-donation)	-29.8 (back-donation)	-31.6 (back-donation)	-15.3 (back-donation)
[a] Values into bracket (%) correspond to the percentage contribution to the total attractive interaction (ΔV_{elstat} + ΔE_{orb}).				

For the best fragmentation, we carried out EDA analysis for **A-Ph**, **A-Mes**, **A-Dmp** and **B-Mes** for comparison. In all cases, the main stabilizing contribution to the ΔE_{int} term comes from the electrostatic term (ΔV_{elstat}) which accounts for ~ 70-75 % of the total attractive interaction energy, while the orbital term (ΔE_{orb}) accounts to ~ 25-30 % to the stabilization.

The Natural Orbital for Chemical Valence (NOCV) extension of the EDA method (see Table S4 and Figure S4) indicates that the orbital interaction (ΔE_{orbi} (ρ)) is primarily due to the donation from the carbene to the metal fragment and that this term is relatively similar in all complexes (ΔE_{orb}(ρ) : –44.7 to –50.7 kcal/mol). The metal to carbene back-donation quite significantly contributes to the stabilization in the gold complexes with (P,P) ligand, with ΔE_{orb}(ρ) ~ 30-35 kcal/mol and much less for **B-Mes** (ΔE_{orb}(ρ): –15.3 kcal/mol).

Comparison of **A-Dmp** and **B-Mes** complexes shows that with the bidentate (P,P) ligand the ΔE_{orb} term associated to the back-donation is twice as large compared to the monodentate Johnphos ligand (**B-Mes**), whereas the donation term is relatively close. This means that the back-donation term is enhanced with (P,P) ligand and contributes primilarly to the stabilisation of the carbene, in addition to steric effects.

Figure S4. Plot of the contours of deformation densities contributions ($\Delta\rho_{orb,i}$) of the main pairwise orbital interaction between L_2Au^+ ligand and carbene, and associated orbital interaction energy contribution ($\Delta E_{orb,i}$ in kcal/mol) for the complex **A-Dmp** (a) and **B-Mes** (b), computed at ZORA-B3LYP/TZ2P level of theory. The charge flow is red → blue ($\Delta\rho < 0$ in red and $\Delta\rho > 0$ in blue). The contour value for density is 0.001 a.u.

a) Donation **Back-donation**

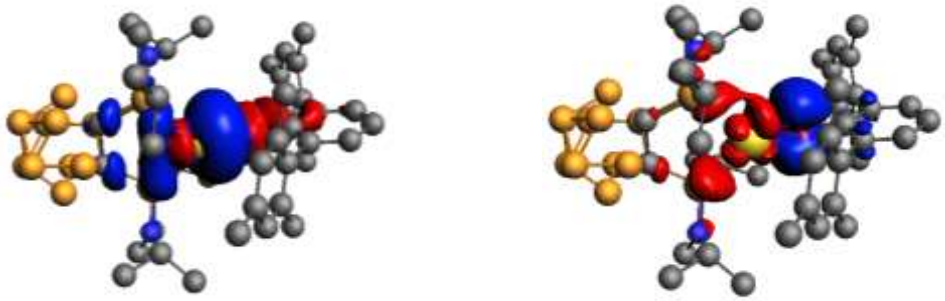

$\Delta E_{orb}(\rho 2)$: –49.6 $\Delta E_{orb}(\rho 1)$: –31.6

b) Donation **Back-donation**

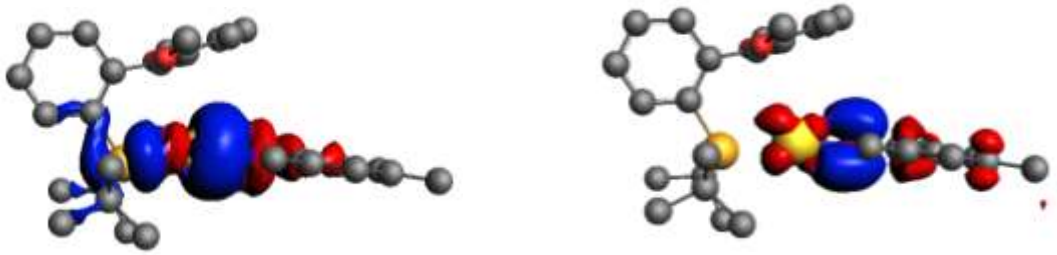

$\Delta E_{orb}(\rho 1)$: –44.7 $\Delta E_{orb}(\rho 2)$: –15.3

References

1) J. E. Borger, A. W. Ehlers, M. L., J. C. Slootweg and K. Lammertsma, *Angew. Chem. Int. Ed.*, 2014, **47**, 12836–12839.

2) V. M. Iluc, C. A. Laskowski and G. L. Hillhouse, *Organometallics,* 2009, **20**, 6135–6138.

3) M. Joost, L. Estévez, S. Mallet-Ladeira, K. Miqueu, A. Amgoune and D. Bourissou, *Angew. Chem. Int. Ed.*, 2014, **52**, 14512–14516.

4) Gaussian 09, M. J. Frisch, G. W. Trucks, H. B. Schlegel, G. E. Scuseria, M. A. Robb, J. R. Cheeseman, G. Scalmani, V. Barone, B. Mennucci, G. A. Petersson, H. Nakatsuji, M. Caricato, X. Li, H. P. Hratchian, A. F. Izmaylov, J. Bloino, G. Zheng, J. L. Sonnenberg, M. Hada, M. Ehara, K. Toyota, R. Fukuda, J. Hasegawa, M. Ishida, T. Nakajima, Y. Honda, O. Kitao, H. Nakai, T. Vreven, J. A. Montgomery, Jr., J. E. Peralta, F. Ogliaro, M. Bearpark, J. J. Heyd, E. Brothers, K. N. Kudin, V. N. Staroverov, T. Keith, R. Kobayashi, J. Normand, K. Raghavachari, A. Rendell, J. C. Burant, S. S. Iyengar, J. Tomasi, M. Cossi, N. Rega, J. M. Millam, M. Klene, J. E. Knox, J. B. Cross, V. Bakken, C. Adamo, J. Jaramillo, R. Gomperts, R. E. Stratmann, O. Yazyev, A. J. Austin, R. Cammi, C. Pomelli, J. W. Ochterski, R. L. Martin, K. Morokuma, V. G. Zakrzewski, G. A. Voth, P. Salvador, J. J. Dannenberg, S. Dapprich, A. D. Daniels, O. Farkas, J. B. Foresman, J. V. Ortiz, J. Cioslowski and D. J. Fox, Gaussian, Inc., Wallingford CT, **2009**.

5) (*a*) A. D. Becke, *Phys. Rev*. 1988, **A38**, 3098–3100; (*b*) A. D. Becke *J. Chem. Phys.* 1993, **98**, 5648–5652; (*c*) J. P. Perdew, in *Electronic Structure of Solids '91*, Ed. P. Ziesche and H. Eschrig, Akademie Verlag, Berlin, 1991, 11.

6) (*a*) D. Andrae, U. Häussermann, M. Dolg, H. Stoll and H. Preuss, *Theor. Chim. Acta,* 1990, **77**, 123–141; (*b*) M. Dolg, *Modern Methods and Algorithm of Quantum Chemistry, Vol. 1* (Ed.: J. Grotendorst), John von Neuman Institute for Computing, Jülich (Germany), 2000, 479.

7) A. W. Ehlers, M. Biihme, S. Dapprich, A. Gobbi, A. Hijllwarth, V. Jonas, K. F. Kiihler, R. Stegmann, A. Veldkamp and G. Frenking, *Chem. Phys. Lett.,* 1993, **208**, 111–114.

8) P. C. Hariharan and J. A. Pople, *Theor. Chim. Acta,* 1973, **28**, 213–222.

9) Chemcraft graphical software for visualization of quantum chemistry computations. https://www.chemcraftprog.com

10) (*a*) E. Reed, L. A. Curtiss and F. Weinhold, *Chem. Rev.,* 1988, **88**, 899–926; (*b*) J. P. Foster and F. Weinhold, *J. Am. Chem. Soc.,* 1980, **102**, 7211–7218; (*c*) A. E. Reed and F. Weinhold, *J. Chem. Phys.,* 1985, **83**, 1736–1740.

11) NBO 7.0 program, E. D. Glendening, J. K. Badenhoop, A. E. Reed, J. E. Carpenter, J. A. Bohmann, C. M. Morales, P. Karafiloglou, C. R. Landis and F. Weinhold, Theoretical Chemistry Institute, University of Wisconsin, Madison, 2018.

12) S. Dapprich and G. Frenking, *J. Phys. Chem.,* 1995, **99**, 9352–9362.

13) (a) K. Morokuma, *J. Chem. Phys.*, 1971, **55**, 1236–1244; (b) T. Ziegler, A. Rauk, *Theor. Chim. Acta*, 1977, **46**, 1–10.

14) (a) G. te Velde, F. M. Bickelhaupt, E. J. Baerends, C. Fonseca Guerra, S. J. A. van Gisbergen, J. G. Snijders and T. Ziegler, *Journal of Computational Chemistry*, **2001**, *22*, 931. (b) ADF 2021.1, SCM, Theoretical Chemistry, Vrije Universiteit, Amsterdam, The Netherlands, http://www.scm.com. (c) E. J. Baerends, T. Ziegler, J. Autschbach, D. Bashford, A. Bérces, F. M. Bickelhaupt, C. Bo, P. M. Boerrigter, L. Cavallo, D. P. Chong, L. Deng, R. M. Dickson, D. E. Ellis, M. van Faassen, L. Fan, T. H. Fischer, C. Fonseca Guerra, M. Franchini, A. Ghysels, A. Giammona, S. J. A. van Gisbergen, A. W. Götz, J. A. Groeneveld, O. V. Gritsenko, M. Grüning, S. Gusarov, F. E. Harris, P. van den Hoek, C. R. Jacob, H. Jacobsen, L. Jensen, J. W. Kaminski, G. van Kessel, F. Kootstra, A. Kovalenko, M. V. Krykunov, E. van Lenthe, D. A. McCormack, A. Michalak, M. Mitoraj, S. M. Morton, J. Neugebauer, V. P. Nicu, L. Noodleman, V. P. Osinga, S. Patchkovskii, M. Pavanello, P. H. T. Philipsen, D. Post, C. C. Pye, W. Ravenek, J. I. Rodríguez, P. Ros, P. R. T. Schipper, H. van Schoot, G. Schreckenbach, J. S. Seldenthuis, M. Seth, J. G. Snijders, M. Solà, M. Swart, D. Swerhone, G. te Velde, P. Vernooijs, L. Versluis, L. Visscher, O. Visser, F. Wang, T. A. Wesolowski, E. M. van Wezenbeek, G. Wiesenekker, S. K. Wolff, T. K. Woo, A. L. Yakovle, **ADF 2021**, SCM, Theoretical Chemistry, Vrije Universiteit, Amsterdam, The Netherlands, http://www.scm.com.

15) M. Mitoraj, A. Michalak, T. Ziegler, *J. Chem. Theor. Comput.* 2009, **5**, 962–975.

NMR Spectra

NMR spectra of DmpI

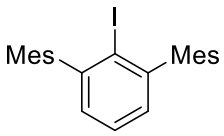

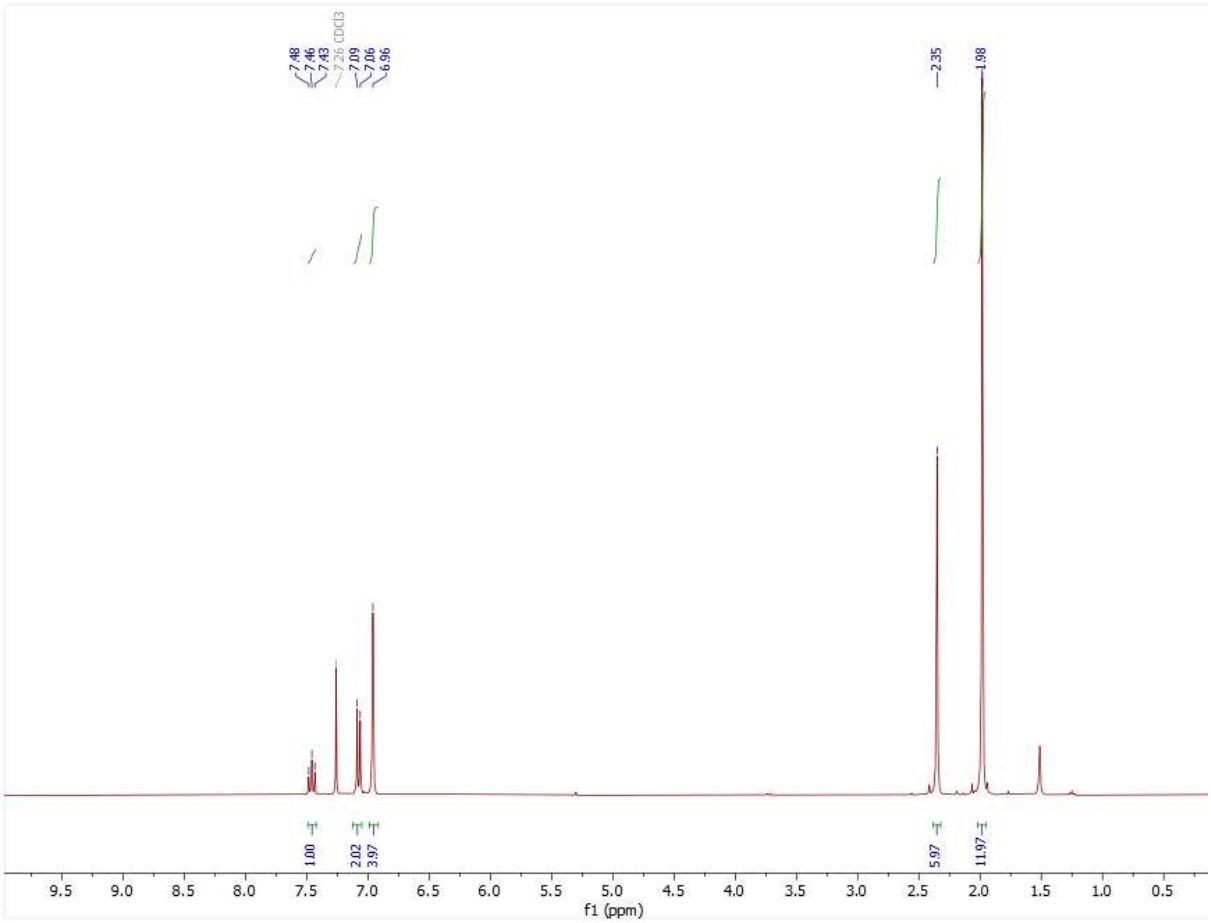

Figure S5. ^{1}H NMR (300.11 Hz, $CDCl_3$) spectrum of dmpI.

NMR spectra of CHODmp

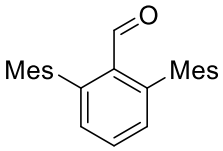

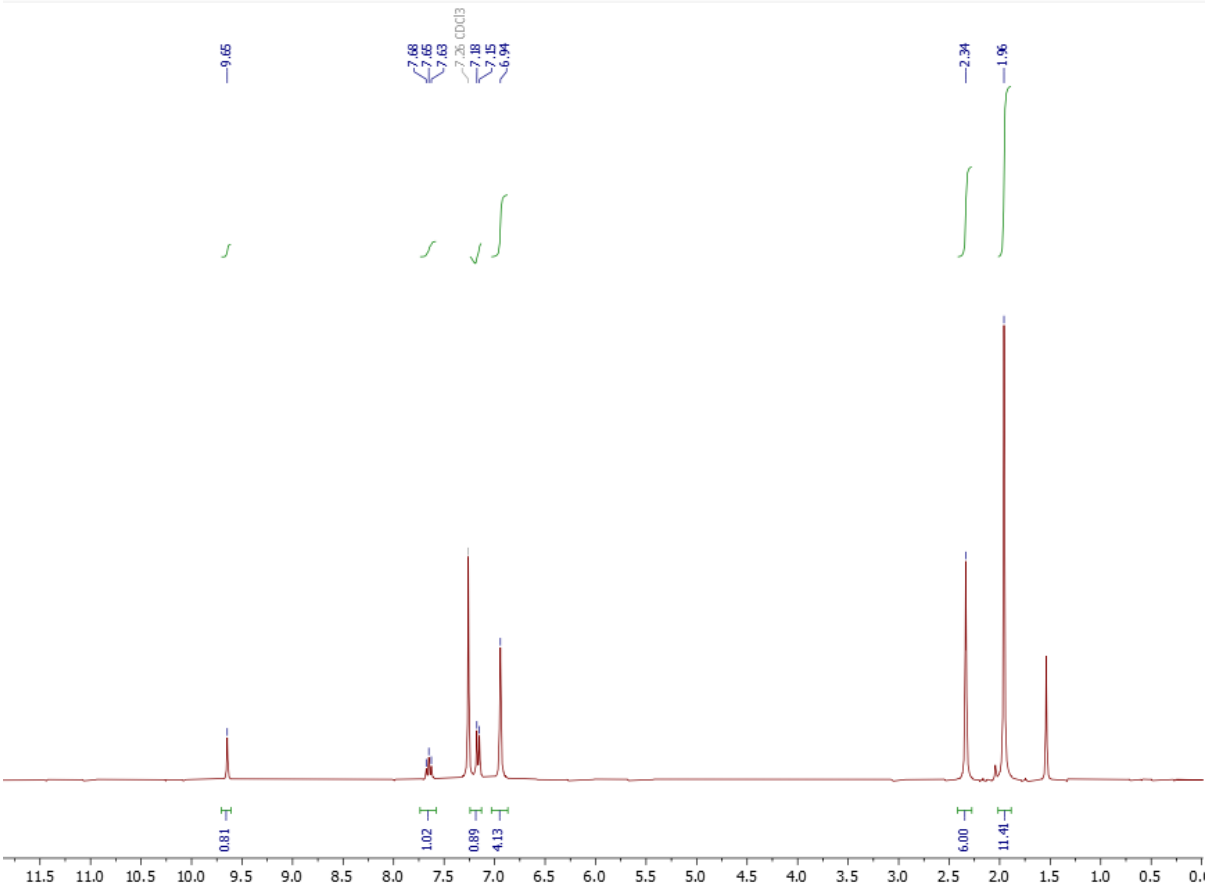

Figure S6. ^{1}H NMR (300.11 Hz, $CDCl_3$) spectrum of CHODmp.

NMR spectra of CH(NNHTs)Dmp

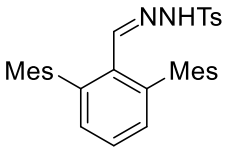

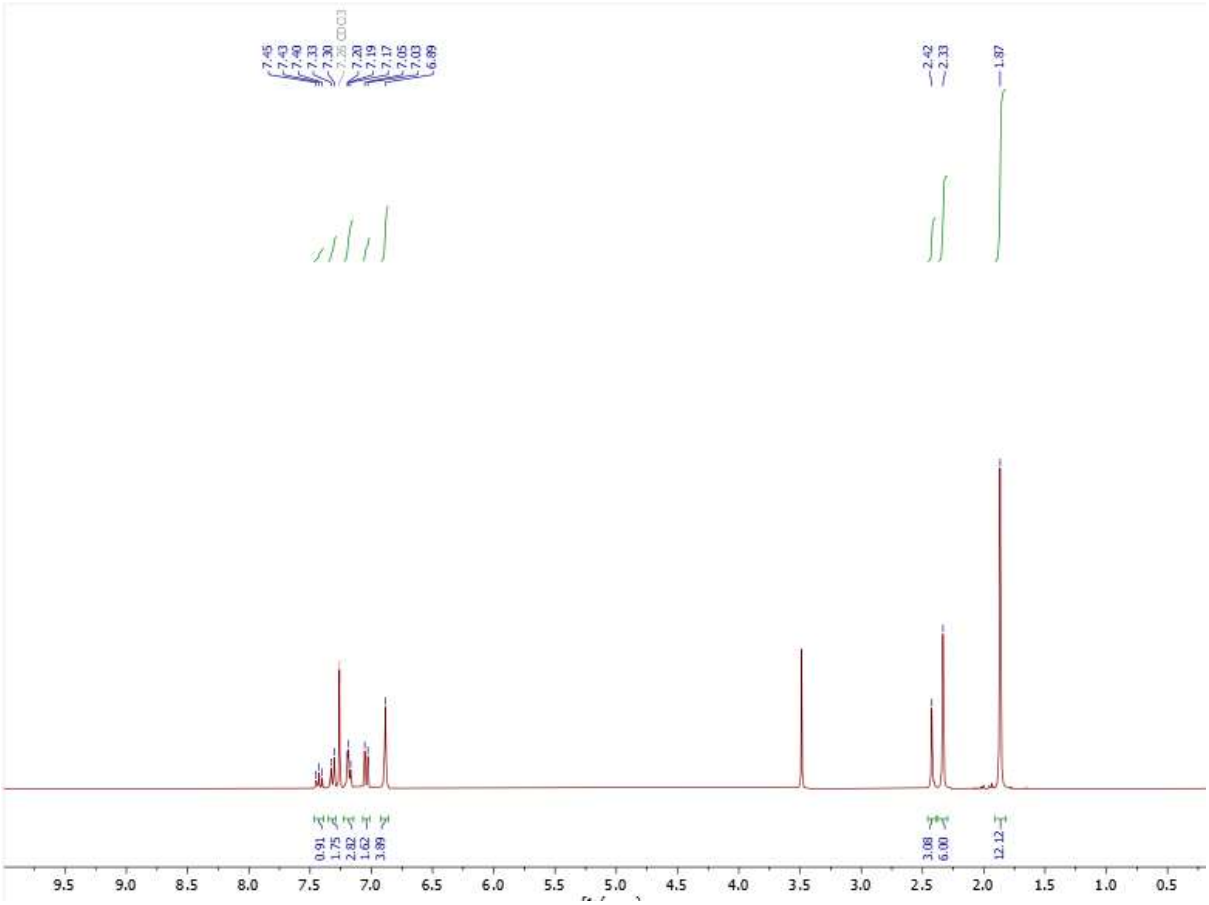

Figure S7. ^{1}H NMR (300.11 Hz, $CDCl_3$) spectrum of CH(NNHTs)Dmp.

NMR spectra of $CH(N_2)Dmp$

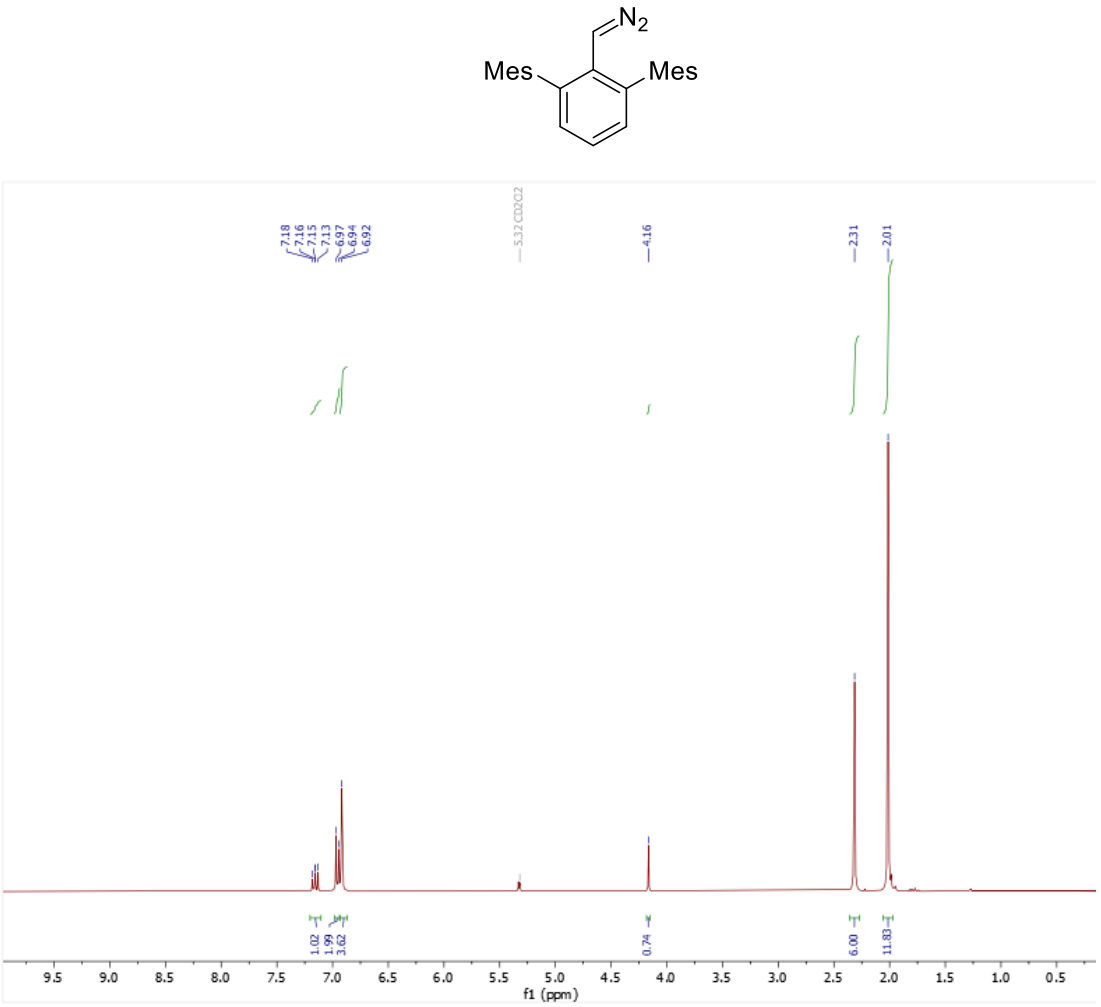

Figure S8. ^1H NMR (300.11 Hz, $CDCl_3$) spectrum of $CH(N_2)Dmp$.

NMR spectra of **1**

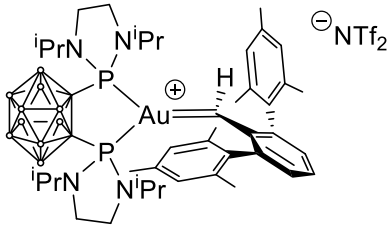

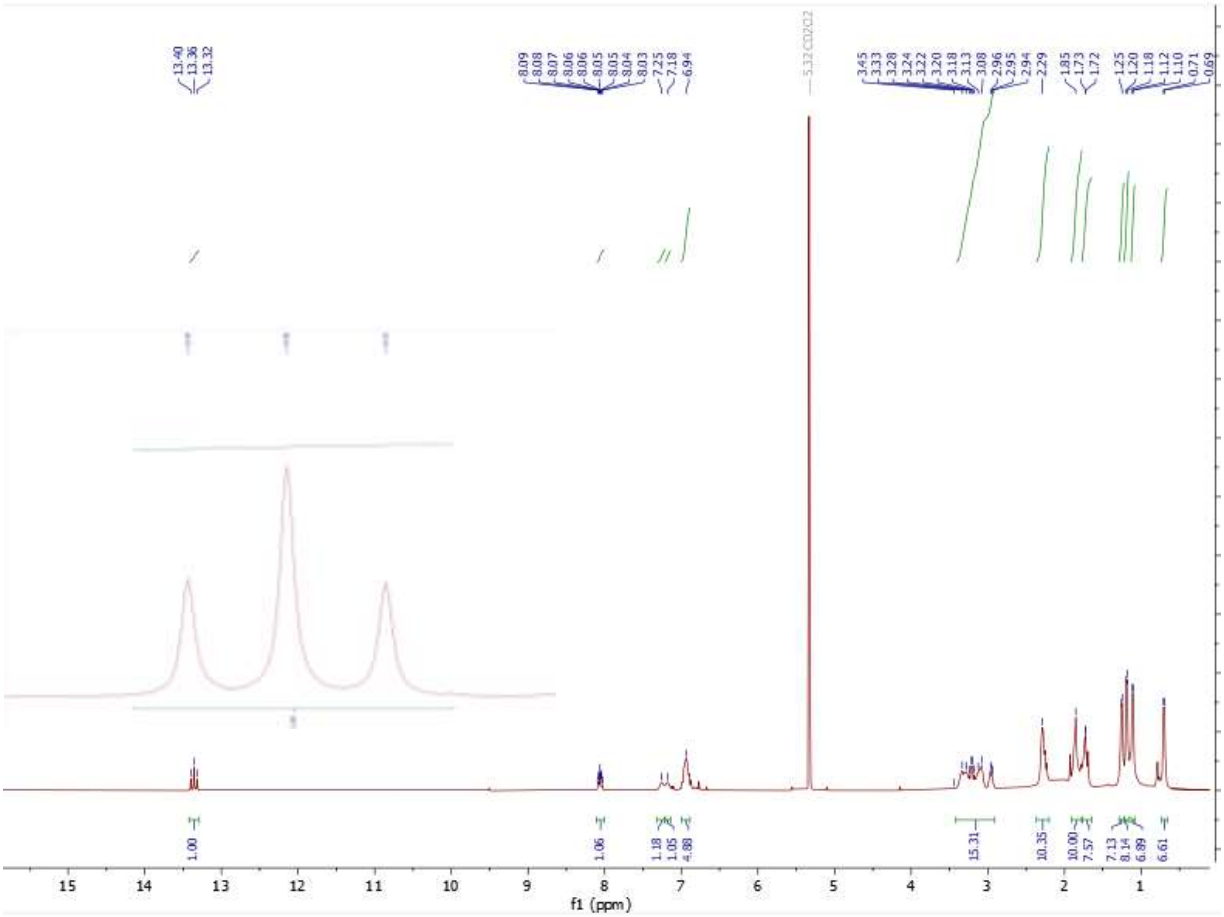

Figure S9. ^{1}H NMR (400.13 Hz, CD_2Cl_2, -80°C) spectrum **1**.

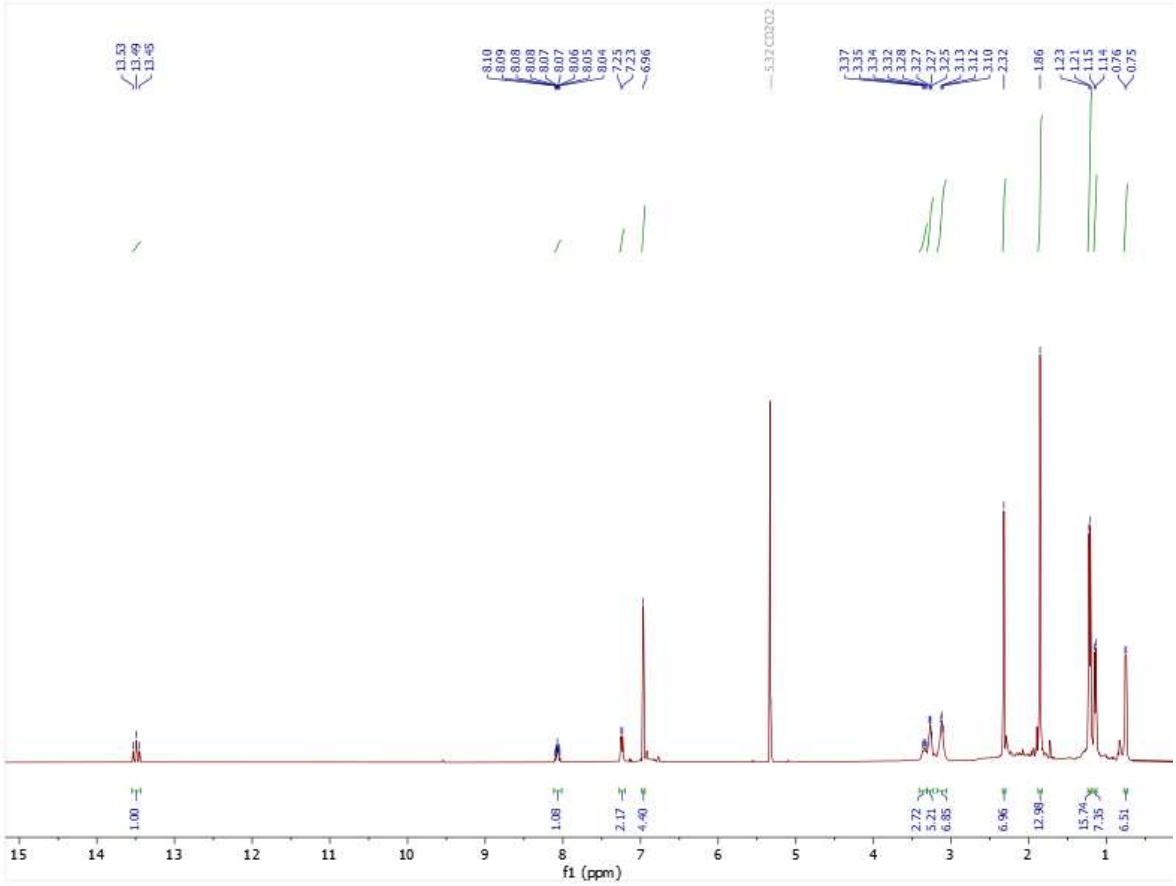

Figure S10. ^{1}H NMR (400.13 Hz, CD_2Cl_2, -30°C) spectrum of **1**.

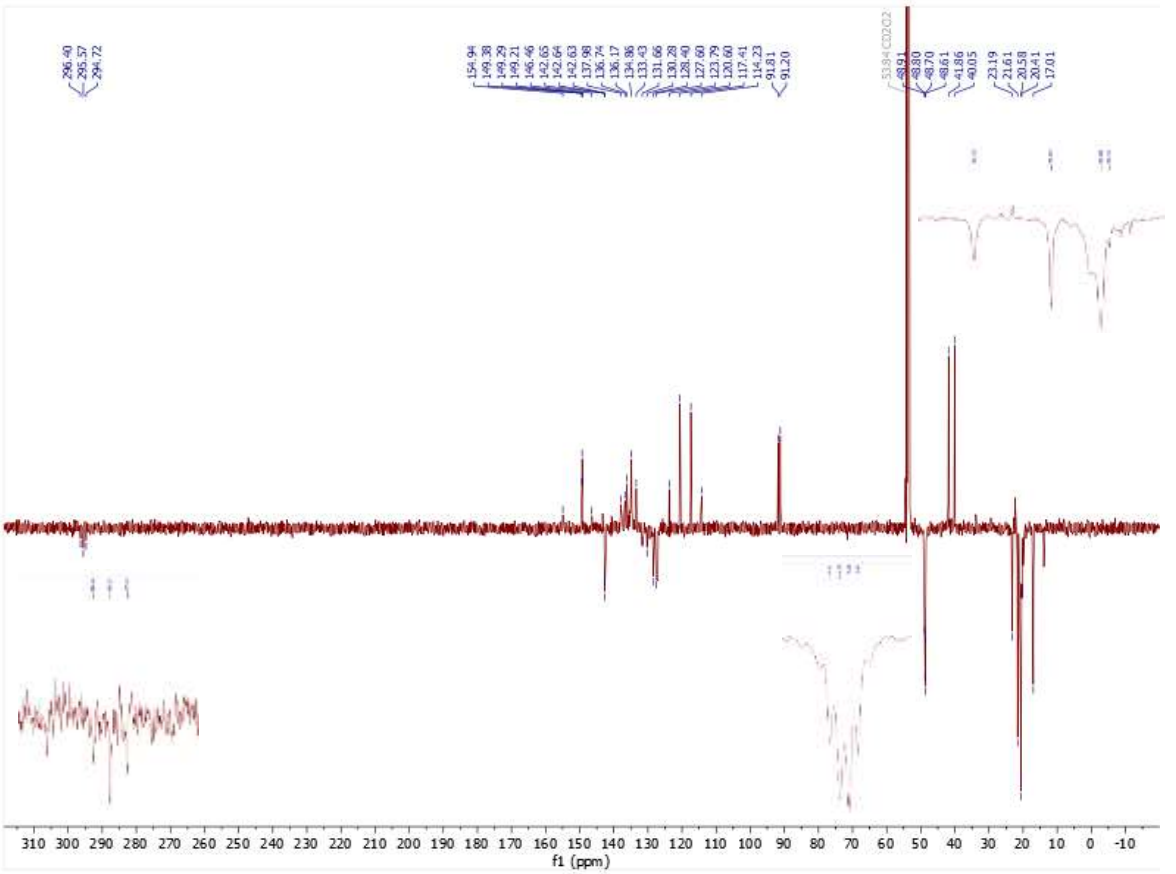

Figure S11. ^{13}C NMR (100.63 Hz, CD_2Cl_2, -80°C) spectrum of **1**.

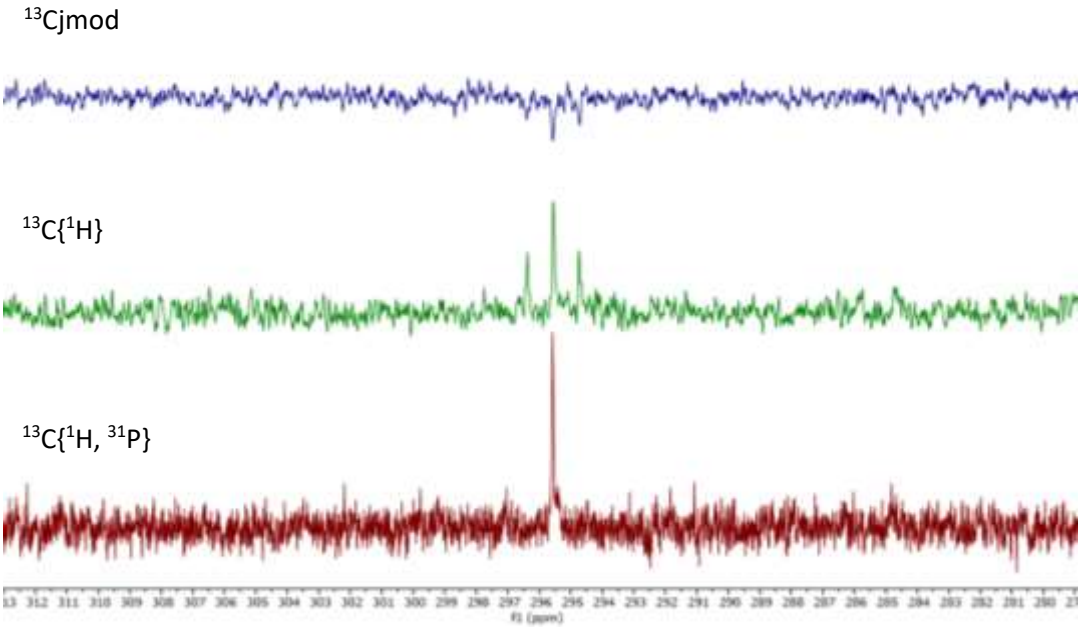

Figure S12. $^{13}C_{Jmoldulate}$ NMR (100.63 Hz, CD_2Cl_2, -80°C), $^{13}C\{^1H\}$ NMR (100.63 Hz, CD_2Cl_2, -80°C)], $^{13}C\{^1H, ^{31}P\}$ NMR (100.63 Hz, CD_2Cl_2, -80°C) spectra of **1**.

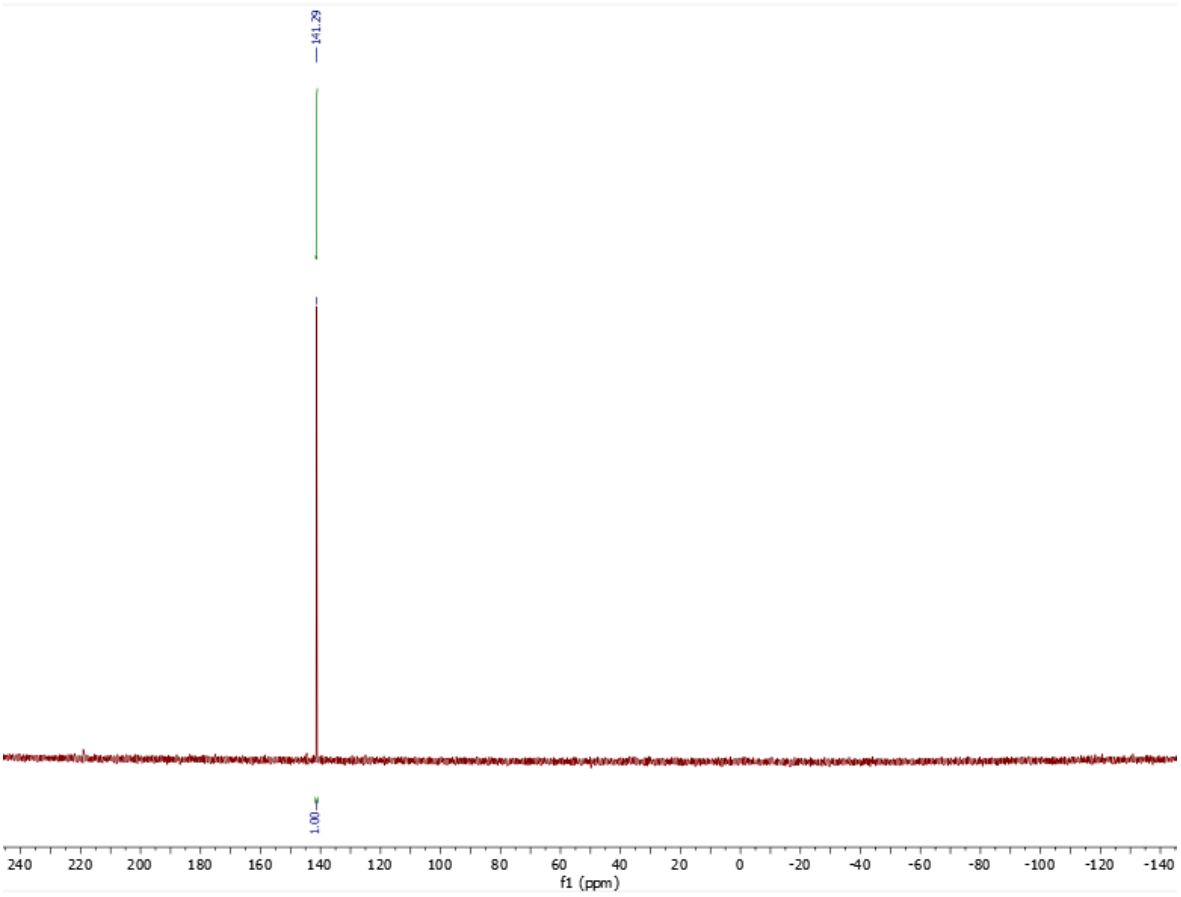

Figure S13. $^{31}P\{^1H\}$ NMR (161.98 MHz, CD_2Cl_2, -80°C) spectrum of **1**.

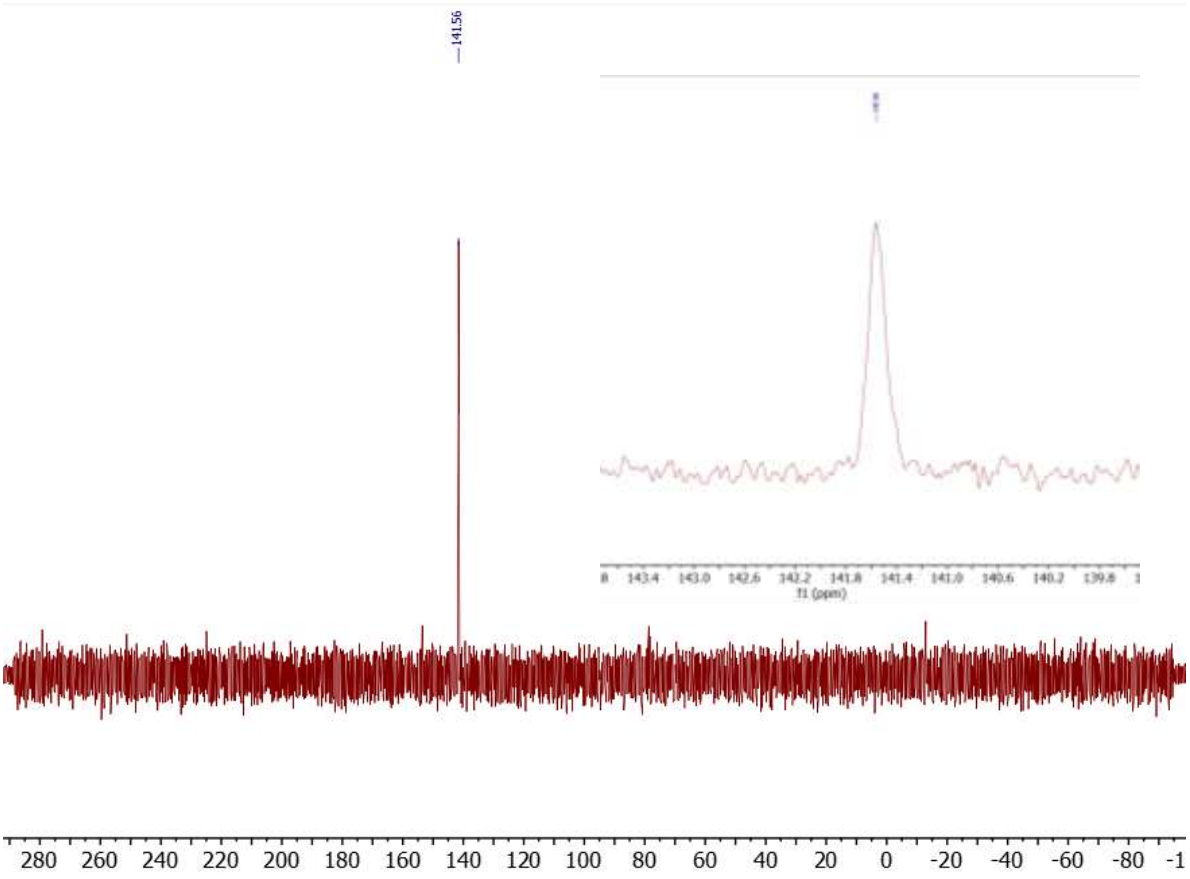

Figure S14. ^{31}P NMR (161.99 MHz, CD_2Cl_2, -80°C) spectrum of **1**.

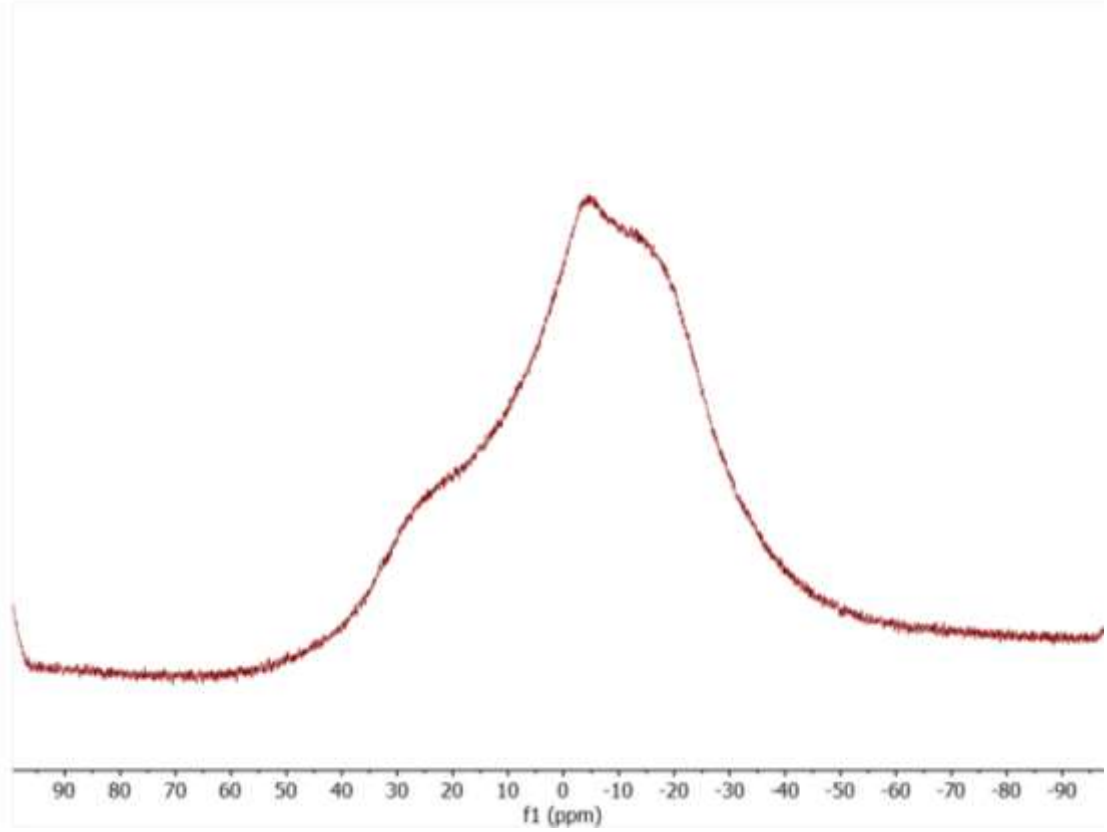

Figure S15. ^{11}B NMR (128.38 MHz, CD_2Cl_2, -80°C) spectrum of **1**.

Variable temperature NMR spectra of **1**

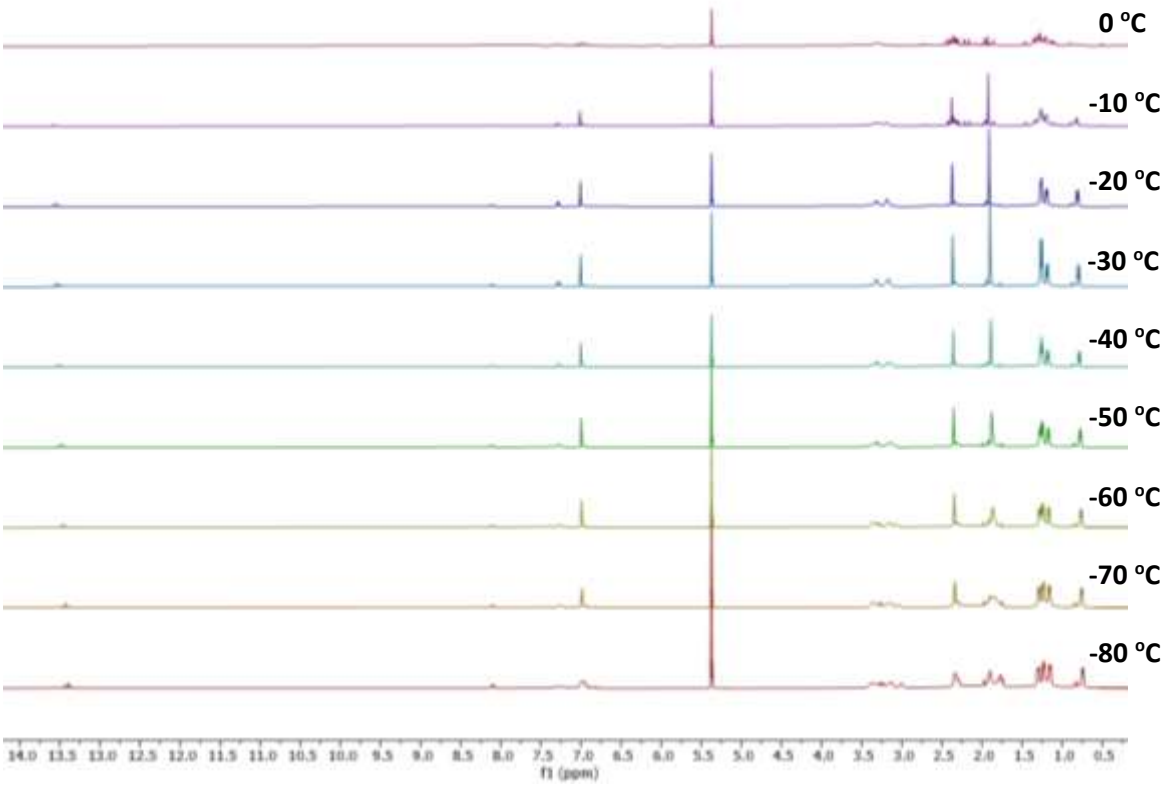

Figure S16. ^{1}H NMR spectra of **1** from -80 °C to 0 °C in increments of 10 °C.

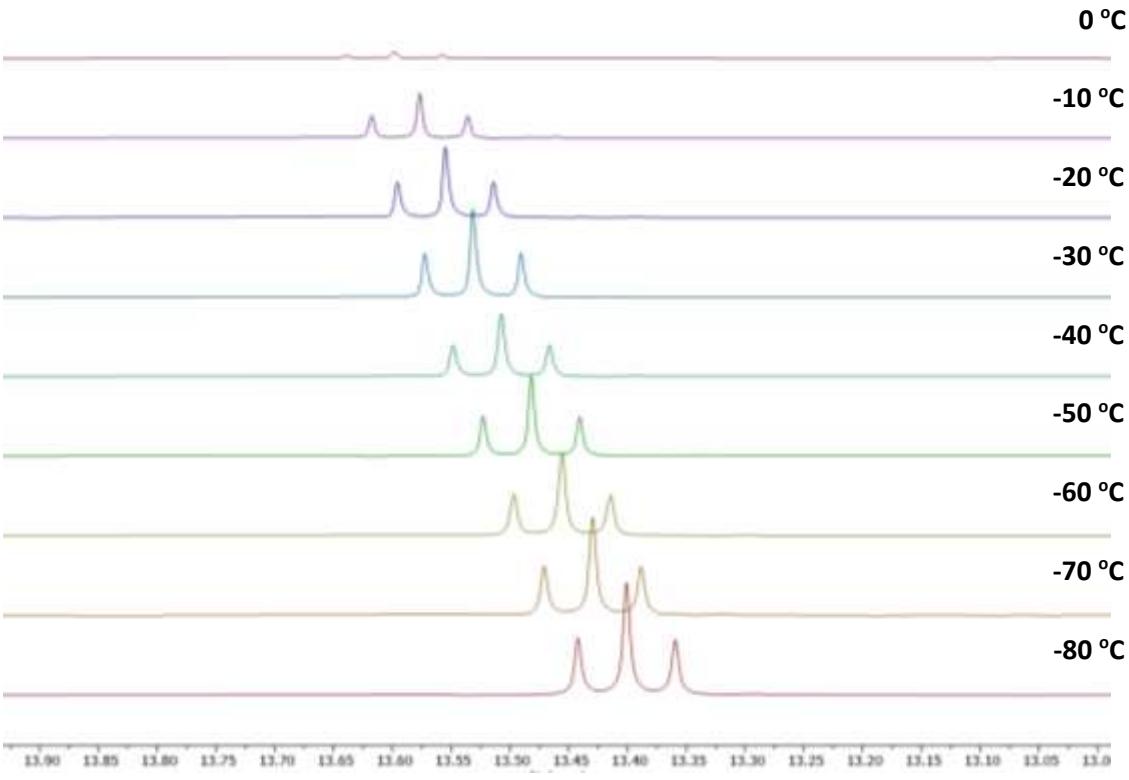

Figure S17. ^{1}H NMR spectra of **1** from -80 °C to 0 °C in increments of 10 °C from 13.0 to 14.0 ppm.

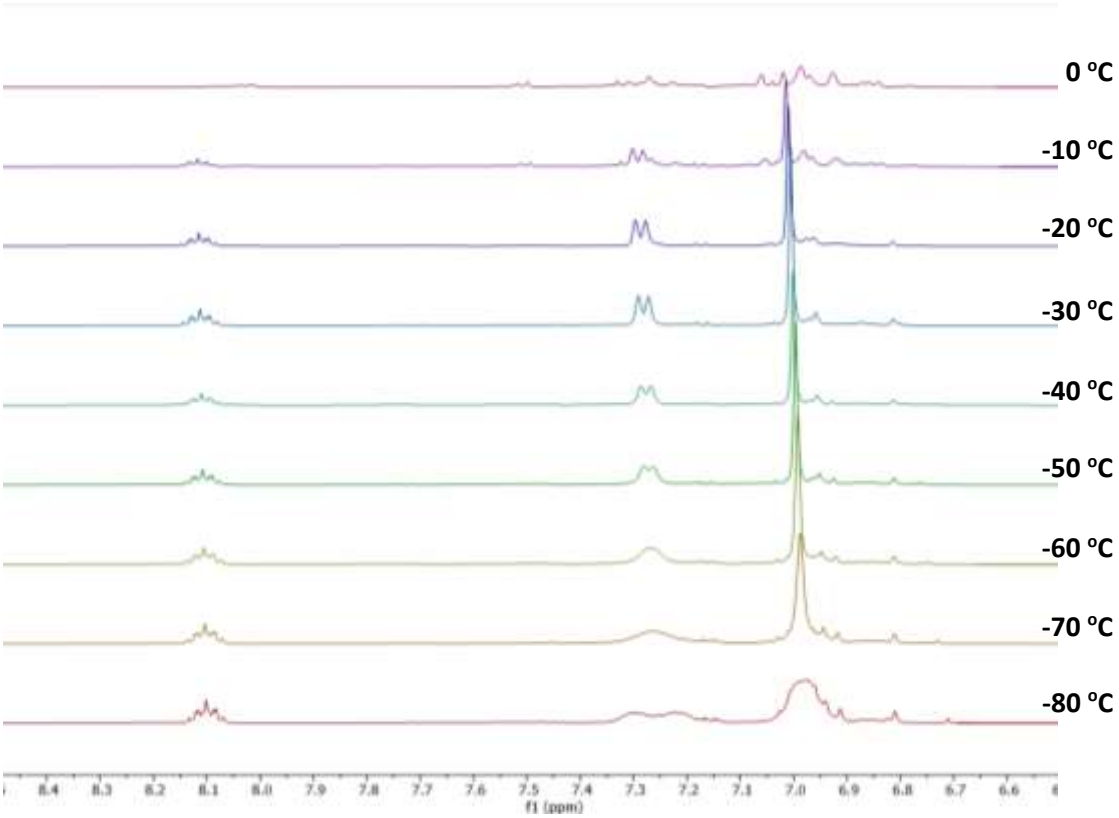

Figure S18. ^{1}H NMR spectra of **1** from -80 °C to 0 °C in increments of 10 °C from 6.5 to 8.5 ppm.

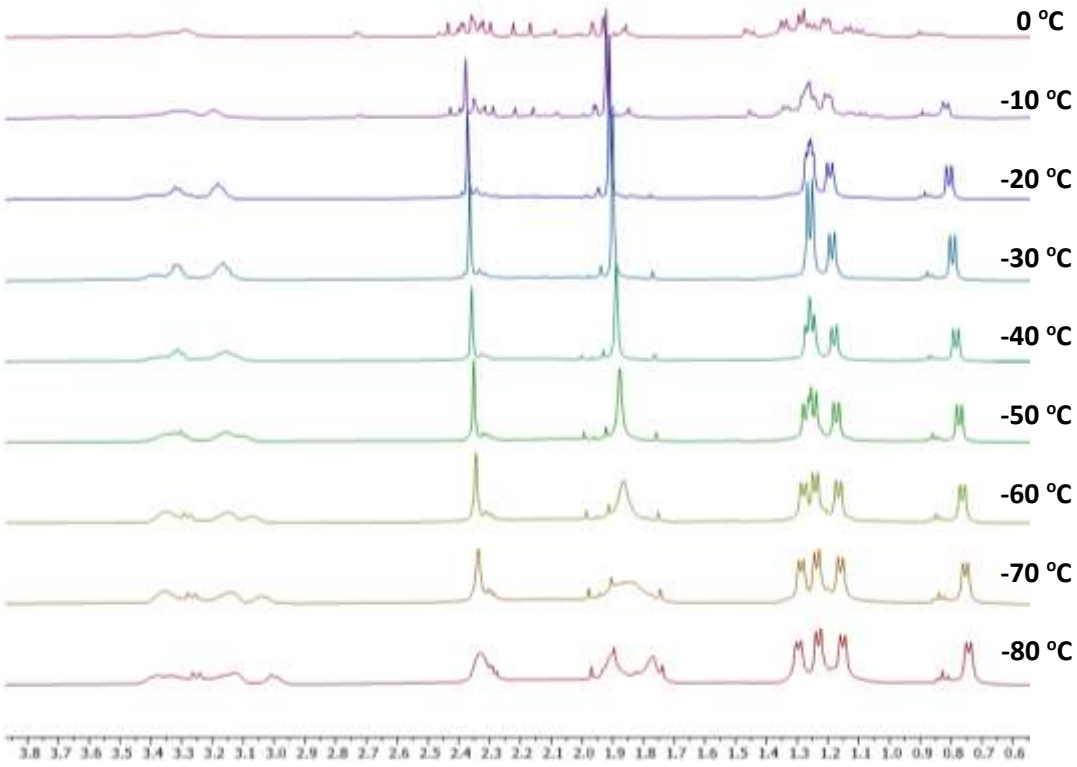

Figure S19. ^{1}H NMR spectra of **1** from -80 °C to 0 °C in increments of 10 °C from 0.5 to 4.0 ppm.

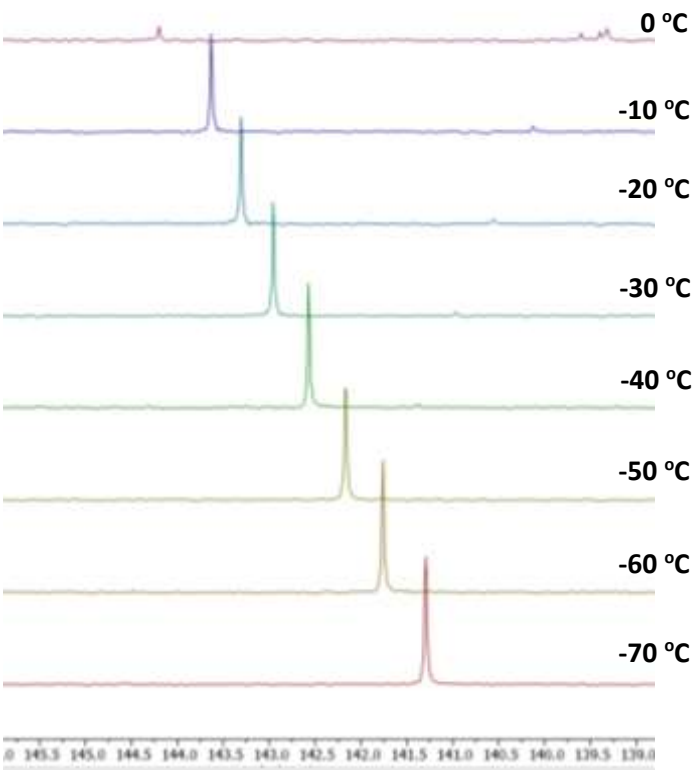

Figure S20. ^{31}P NMR spectrum of **1** from -70 °C to 0 °C in increments of 10 °C from 139 to 145 ppm.

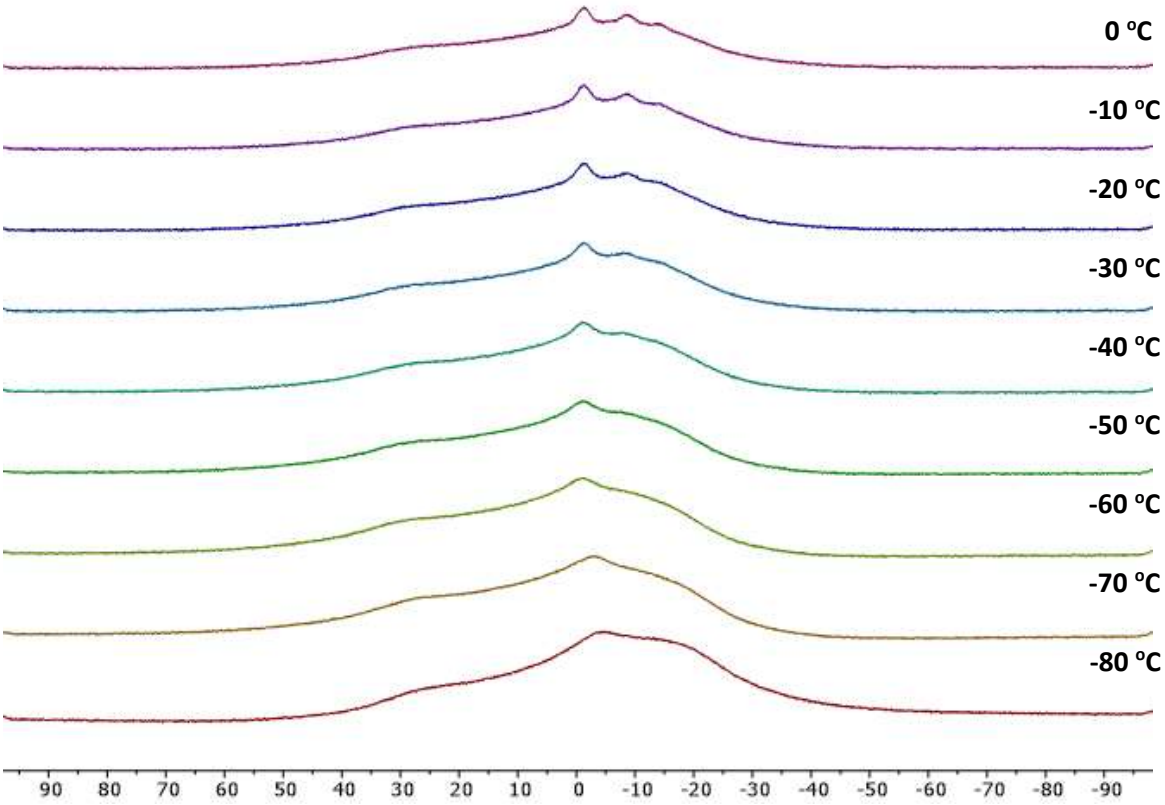

Figure S21. ^{11}B NMR spectrum of **1** from -80 °C to 0 °C in increments of 10 °C.